EPJ E
Soft Matter and Biological Physics
EPJ.org
your physics journal

Eur. Phys. J. E (2015) **38**: 18 DOI 10.1140/epje/i2015-15018-3

# Tunable diffusive lateral inhibition in chemical cells

Ning Li, Nathan Tompkins, Hector Gonzalez-Ochoa and Seth Fraden

edp sciences Società Italiana di Fisica Springer

Eur. Phys. J. E (2015) **38**: 18
DOI 10.1140/epje/i2015-15018-3

THE EUROPEAN PHYSICAL JOURNAL E

Regular Article

# Tunable diffusive lateral inhibition in chemical cells*

Ning Li[1], Nathan Tompkins[1], Hector Gonzalez-Ochoa[1,2], and Seth Fraden[1,a]

[1] Department of Physics, Brandeis University, Waltham, MA 02454, USA
[2] Department of Applied Mathematics, IPICYT, San Luis Potosi, Mexico

Received 9 October 2014 and Received in final form 7 February 2015
Published online: 23 March 2015 – 

**Abstract.** The Belousov-Zhabotinsky (BZ) reaction has become the prototype of nonlinear chemical dynamics. Microfluidic techniques provide a convenient method for emulsifying BZ solutions into monodispersed drops with diameters of tens to hundreds of microns, providing a unique system in which reaction-diffusion theory can be quantitatively tested. In this work, we investigate monolayers of microfluidically generated BZ drops confined in close-packed two-dimensional (2D) arrays through experiments and finite element simulations. We describe the transition from oscillatory to stationary chemical states with increasing coupling strength, controlled by independently varying the reaction chemistry within a drop and diffusive flux between drops. For stationary drops, we studied how the ratio of stationary oxidized to stationary reduced drops varies with coupling strength. In addition, using simulation, we quantified the chemical heterogeneity sufficient to induce mixed stationary and oscillatory patterns.

## 1 Introduction

Alan Turing's work on morphogenesis in cells, although more than 60 years old, continues to motivate and inspire theoretical and experimental biologists [1]. That said, there are very few experimental systems for which Turing's theory of reaction-diffusion (RD) in cells is applicable. While numerous examples in biological tissue patterning, such as lateral inhibition between contacting cells in Delta-Notch signaling [2–4] resemble the reaction-diffusion systems Turing proposed, only a very limited set of biological patterns have been established to be based on RD Turing instabilities [5,6]. Therefore the Turing model is regarded more as a metaphor for pattern formation than as a model suitable for prediction and quantitative comparison with experiment.

The Belousov-Zhabotinsky (BZ) reaction, the metal ion catalyzed oscillatory oxidation of an organic substrate by acidic bromate, has become the prototype of nonlinear chemical dynamics [7]. We have demonstrated previously that microfluidically produced emulsions of BZ solution are a convenient experimental chemical system which exhibits multiple phenomena that can be semi-quantitatively explained by Turing's RD mechanism [8]. Microfluidic techniques provide a method for emulsifying BZ solution into monodispersed droplets with the dimensions of tens to hundreds of microns. The diffusive coupling of the chemical species acting as activators and inhibitors between BZ aqueous droplets suspended in a continuous oil media render the BZ emulsion system highly suitable for the study of synchronization and pattern formation in networks of coupled nonlinear chemical oscillators.

Previously [8–11] we investigated in detail the behavior of linear arrays of BZ droplet and also analyzed several dynamical patterns observed in monolayers of BZ droplets confined in close-packed two-dimensional (2D) arrays [12]. In this paper we examine 2D arrays of drops in more detail through experiments and finite element simulations. We describe the transition from oscillatory to stationary chemical states with increasing coupling strength. For drops in the stationary state, we study how the ratio of stationary oxidized to stationary reduced drops increases with coupling strength. We also provide simulation results to address a previously unresolved question [8]: what amount of chemical heterogeneity among BZ drops is sufficient to generate mixed oscillatory and stationary patterns?

## 2 Methods

BZ emulsions were generated using a flow focusing microfluidic technique as described in our previous work [10]. The oil used in this work is a perfluorinated oil, HFE 7500 (3M Corp.). Since this is the only oil used, we will refer to it as "the oil". An amphiphilic PEG-PFPE fluorinated block copolymer dissolved at a concentration of 2% by

* Supplementary material in the form of six .mpg files, one .png and one .mph file available from the Journal web page at `http://dx.doi.org/10.1140/epje/i2015-15018-3`

[a] e-mail: `fraden@brandeis.edu`

volume in the oil serves as a surfactant for aiding droplet formation and preventing droplet coalescence. The surfactant was provided by RainDance Technologies (Lexington, MA, USA) and is similar to a surfactant described in the literature [13]. We note that a very satisfactory alternative is now commercially available (RAN Biotechnologies, Inc.). Rectangle glass capillaries (VitroTubes$^{TM}$) were directly used for 2D emulsion storage without further treatment. The capillaries were either 50, 100 or 200 $\mu$m in height, chosen to be somewhat smaller than the droplet diameter such that the emulsion would spontaneously form a monolayer. The capillary widths were either 10 or 20 times the height and the capillary lengths were hand cut between 2 to 4 cm. Such a capillary filled with BZ emulsion can be effectively treated as a 2D system whose height is much smaller than the other two dimensions. Inside the capillary, monodispersed micro-droplets stabilized by the surfactant spontaneously form a close-packed hexagonal lattice so that the system is at the highest packing density. The capillaries were positioned so that the normal of the plane defined by the capillary width and length was oriented parallel to gravity.

Detailed descriptions of chemical preparation and our home-made optical system for illumination and data recording can be found in previous works [8–10]. Our BZ mixture in droplets consisted of the following: $[H_2SO_4]$ = 80 mM, [NaBr] = 10 mM, $[NaBrO_3]$ = 300 mM, [Ferroin] = 3 mM and $[Ru(bipy)_3]$ = 0.4 mM. Both metal catalysts were in the reduced form. This recipe was used in our experiments with various malonic acid concentrations, [MA], or $m$ for short, which was the only tunable parameter in our BZ chemistry.

The theoretical model used in this paper for the BZ reaction chemistry is identical to the one in previous works [9,10], which is the well established 7-variable FKN model [14,15] with minor modifications [16,17]. For the sake of completeness, the equations are included in appendix A. Coupling from one drop to another through the intervening oil was realized in the model by allowing up to three chemical species to partition into the oil with an appropriate permeation constant. No chemical reactions were considered to occur in the oil phase and the chemical species in the oil moved according to Fick's laws of diffusion. The 2D reaction-diffusion equation was solved using the finite element solver COMSOL multiphysics®. An example of the COMSOL code is included in Supplementary material S1. Periodic boundary conditions were used with different numbers of drops in the unit cell. The three species which were allowed to partition into the oil phase were the non-polar species bromine ($Br_2$), which acts as the sole inhibitor, and the radical $BrO_2\cdot$ and weakly polar bromous acid $HBrO_2$, both of which act as activators. The fluorinated HFE oil we used is almost apolar, thus an apolar molecule partitions preferably into the oil phase rather than the aqueous phase. The partition coefficients, the ratio of concentration at equilibrium in the oil phase to the aqueous phase at the oil/water interface, used in the simulation are: $P_B = 2.5$ for bromine, $P_R = 1$ for the radical, and $P_H = 0.01$ for bromous acid.

In order to explore which of the species is most important for coupling, simulations with various combinations of coupling species including bromine only coupling ($P_B = 2.5$, $P_R = P_H = 0$), bromine and radical coupling ($P_B = 2.5$, $P_R = 1$, $P_H = 0$), as well as coupling with all three species were performed for a wide range of values of two parameters which controlled coupling strength; malonic acid concentration ($m$) and drop diameter ($a$).

The purpose of introducing the concept of coupling strength between BZ droplets is to develop a qualitative and quantitative understanding of the physical and chemical factors that control synchronization of BZ drops. The chemical concentrations of a single oscillating drop execute a limit cycle, which is a closed, stable trajectory in the space of chemical concentrations. When two drops are weakly coupled, each drop stays on the same limit cycle but the drops synchronize, either in-phase or $\pi$ radians out-of-phase. We offer two experimental criteria for measuring coupling strength. One experiment to define coupling strength is to consider two drops which initially begin to oscillate with a phase difference that is different than their steady state phase difference and measure the time it takes to reach steady state [8]. The inverse of this time is the synchronization rate, which can be considered to be a measure of coupling strength. For BZ emulsions the synchronization rate increases as either the drop size or separation is decreased leading to the conclusion that coupling strength increases as drop size or separation decreases.

As coupling strength between two drops is increased beyond a certain point, the drops stop oscillating. This can happen abruptly with little change in the limit cycle before the oscillatory to stationary transition. Therefore the transition from a limit cycle to a fixed point is a second convenient experimental method to demarcate the border between weak and strong coupling. For example, for one set of chemical conditions a pair of drops separated by a large interdrop distance may both be oscillating, but as the separation between the drops is decreased, the drops turn stationary. Thus, we conclude that coupling strength increases as interdrop separation decreases.

Previous studies identified bromine as the dominant chemical species which diffuses between drops [11]. Bromine itself functions as a communicator of inhibition and not the inhibitor itself in the following fashion. Bromine, being apolar, readily partitions from the BZ solution into the oil phase. Once inside a neighboring drop, bromine reacts with malonic acid to form bromo-malonic acid and bromide, the latter of which acts as an inhibitor in the BZ reaction, serving to hold the system in the reduced state. Because bromide is charged, it is insoluble in the oil. If the malonic acid concentration is high, then adding bromine has little effect on the chemical dynamics for two reasons, according to previous numerical studies [9]. First, high malonic acid concentration leads to high $Br_2$ consumption inside a drop, leaving less $Br_2$ to diffuse between drops. Second, at high malonic acid concentration, the $Br_2$ that is emitted from one drop and transported through the oil is rapidly consumed in the receiv-

ing drop upon arrival and therefore only slightly increases the $Br_2$ concentration in the receiving drop.

One heuristic measure of the coupling strength between drops in contact is the dimensionless number [8,9]

$$S = \alpha P_B D/(a^2 k_{\text{eff}}) = \mu/k_{\text{eff}}, \quad (1)$$

where $P_B$ is the partition coefficient of bromine, $D$ is the diffusion coefficient of bromine, $a$ is the BZ droplet size and $\alpha$ is a numeric factor of order 10 for drops whose surfaces are separated by a surfactant layer of thickness $10^{-4}a$. The dimensionless coupling strength $S$ is the ratio of two rates: $\mu = \alpha P_B D/a^2$, the rate of diffusive transport between BZ drops of the inhibitor bromine in the limit of a small oil gap [8], and $k_{\text{eff}}$, the effective rate constant characterizing the consumption of $Br_2$, which occurs *via* bromination of malonic acid [9]. Our previous numerical studies suggest that $k_{\text{eff}} \propto m$ [9]. The derivation of $\mu$ is presented elsewhere [8]. The dimensionless ratio of reaction rate to diffusive rate is known as the Damköhler number (Da), used in chemical engineering to assess the degree of conversion in a continuous stirred-tank reactor, while $S$ is the inverse. Large coupling strength corresponds to $S \gg 1$ and occurs when the drops are small and/or the malonic acid concentration is low. When the coupling strength is large, more bromine is transferred between drops than can be consumed and therefore the chemical concentration of each drop is influenced by the other. On the other hand, when the coupling is weak, the amount of bromine transferred is small enough to be rapidly consumed and thus the drops are insensitive to each other's presence [9].

## 3 Results

### 3.1 Tunable diffusive lateral inhibition

We borrow the term "lateral inhibition" from biology to describe the effect of interdrop diffusion of bromine on the oscillation of BZ droplets. In the BZ reaction, the oxidized state is the result of an autocatalytic process and can be considered the "active" state, while the reduced state can be considered "inhibited". In the stationary state, a pair of initially identical drops spontaneously differentiates chemically to a state in which one is oxidized and produces the inhibitor bromine and the other is reduced and absorbs the bromine.

Drop diameter $a$ and malonic concentration $m$ are the two parameters we tune to change coupling strength. Figure 1a is an experimental state diagram of oscillation patterns for a monolayer of monodispersed BZ droplets close-packed in a hexagonal array, as a function of drop diameters at a constant malonic acid concentration of 640 mM. The unit cell of the hexagonal array consists of three drops. The diagram shows the fraction of droplets in one of three states; the oscillating state shown in green (Osc) or one of two possible stationary states as a function of droplet diameter. Stationary states are either in the oxidized stationary Turing state, shown in blue (OST) or

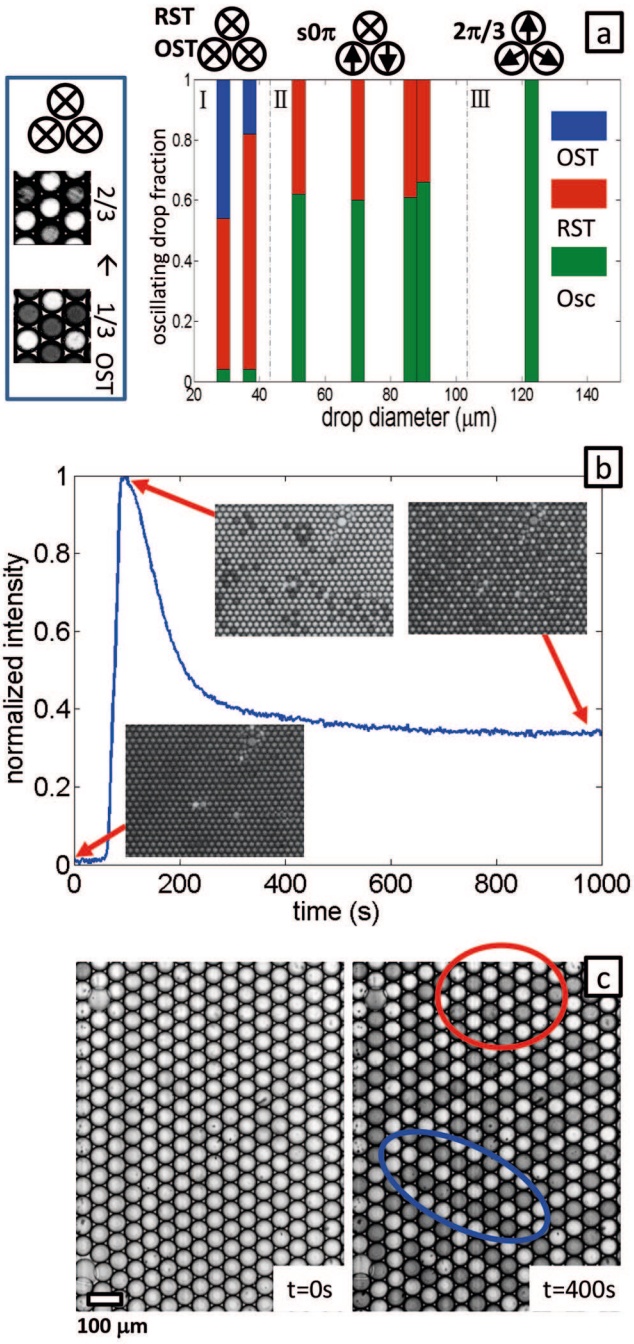


**Fig. 1.** Observed chemical states in 2D hexagonal lattices of BZ drops as a function of drop diameter and malonic acid concentration. a) Patterns as a function of droplet diameter $a$, with $m = 640$ mM. The unit cell has three drops. Arrows denote oscillating drops. The angle between arrows is equal to the phase shift between oscillating drops. The "×" denotes a stationary drop. Inset: Stationary pattern with 2/3 drops oxidized, in comparison to a stationary pattern with 1/3 drops oxidized. b) Stationary Turing pattern with $m = 600$ mM and $a = 50\,\mu$m. The normalized intensity of the drops was plotted as a function of time. The raw data is included in the Supplementary movie S2. c) Stationary Turing pattern with $m = 200$ mM and $a = 50\,\mu$m. The pattern at the moment when all drops first oxidize simultaneously (arbitrarily labeled as $t = 0$) and the stable pattern, 400 seconds later, are shown side by side.

the reduced stationary Turing state, shown in red (RST). Each vertical bar shown in fig. 1a as proportionally colored bars in green (Osc), blue (OST) and red (RST) represents one experiment with several hundreds of identically sized droplets. For a given experiment, only the drops with six nearest neighbors were counted, hence those drops at system boundaries or at lattice defects were omitted. The fraction of drops in each stationary state was normalized by the total number of drops counted in each experiment.

Region III of fig. 1a represents experiments with large drop diameters where the interdrop diffusive coupling is weakest. A series of monodisperse drop arrays were studied in the range 100–450 $\mu$m, although only those with diameter less than 150 $\mu$m are shown in fig. 1a. In region III, all of the drops are oscillating, exhibiting the $2\pi/3$ pattern [12] where each of the three drops in a unit cell oscillates 120 degrees out of phase with each other. This pattern is represented by an icon of 3 circles in a triangle with the arrows' directions indicating the evenly separated phase of the oscillating drops. For a video of the $2\pi/3$ pattern see, Supplementary movies S3, S4 and S5. In region II, corresponding to drops of 50–100 $\mu$m diameter, approximately 2/3 of the drops are oscillating and 1/3 are in the reduced stationary Turing state, in a pattern denoted $s0\pi$ [8] where the nomenclature describes the state of the three drops; one of the three drops in a unit cell is stationary ($s$), and the other two are oscillating $\pi$ radians with respect to each other ($0\pi$). Parenthetically, we note that in another instance we referred to this same pattern as the $\pi$-$s$ state [12]. In several figures this pattern is represented by a triangle of three circles with two arrows in opposite directions representing the 180 degree phase shift between oscillating drops and one with an X representing the one stationary drop. For a movie of the $s0\pi$ state, see Supplementary movie S6 of ref. [8].

Next we report a new phenomenon shown in region I, which is that for even smaller drops, corresponding to stronger coupling strength, almost all the drops enter stationary Turing states and that the fraction of stationary oxidized drops increases as the drop size is decreased. In region I of fig. 1a, corresponding to drops of high malonic concentration ($m = 640$ mM) and less than 50 $\mu$m diameter, most of the drops do not oscillate. Data with two drop sizes were shown in this range. At 40 $\mu$m about 20% were in the oxidized stationary state and about 80% of the drops were in the reduced stationary state. At 30 $\mu$m almost 50% of the drops were oxidized stationary and 50% were reduced stationary. As the diffusive bromine inhibition strength between drops increases with decreasing droplet diameter, we hypothesize that stronger inhibitory coupling leads to a larger fraction of stationary oxidized drops.

Figures 1b and c lend further credence to our hypothesis that bromine coupling strength controls the fraction of oxidized to reduced stationary drops. Here we compare arrays of drops with similar droplet diameter ($\sim 50\,\mu$m) and very different malonic concentrations (600 mM for fig. 1b and 200 mM for fig. 1c). The vast majority of drops in both figs. 1b and c were in the stationary Turing state and resembled the samples shown in region I of fig. 1a.

Figure 1b shows the normalized intensity of more than a thousand droplets as a function of time. Photographs of a small portion of the full field of view were taken at different times. A video of the experiment is shown in Supplementary movie S2. At the very beginning of the experiment, $t = 0$, all drops were near the reduced state (*i.e.* process A in the FKN mechanism, see appendix A) and hence the intensity of the full field of view was the darkest in the whole experiment. This is a consequence of how the samples were prepared. The drops were created with 10 mM bromide to elongate the induction time before the first oscillation. This is convenient to allow us ample time to form the emulsion, seal the sample cells, and adjust the microscope before oscillations start. The intensity of the image during the induction period was set to 0 for normalization. Shortly after the beginning of oscillations, when $t = 94$ s, almost all the drops suddenly transitioned to the oxidized state and the total intensity reached maximum. This intensity was set to 1 for normalization. This initial simultaneous transition to the oxidized state for almost all drops was not a result of synchronization by interdrop communication. Rather it occurred because all the drops were produced with the same composition and at nearly the same time. With time, a fraction of oxidized drops relaxed back to the reduced stationary state and eventually only $\sim 1/3$ drops remained at the oxidized stationary Turing state. The pattern became stable after $t \simeq 400$ s. The stable pattern over a large domain of drops consisted of each oxidized stationary drop surrounded by 6 reduced stationary drops, giving on average 2 reduced (dark) drops for each oxidized (bright) drops, leading to a steady state intensity of 1/3 the maximum value. This pattern is similar to that observed with the 40 $\mu$m diameter drops at 640 mM malonic acid shown in fig. 1a, with a similar fraction of oxidized stationary droplets. Defects in the pattern of oxidized and reduced drops are seen in fig. 1b and Supplementary movie S2. Whether or not the defects are due to random fluctuations or arise as effects of packing imperfections and boundary conditions is unknown.

Figure 1c shows photographs of the initial and the stable state of an array of 50 $\mu$m diameter drops with a lower malonic acid concentration ($m = 200$ mM) than in fig. 1b. At the beginning of recording, almost all drops were in an oxidized state and appeared similar to the photo in fig. 1b at $t = 94$ s. Additionally, in a similar fashion to fig. 1b, after 400 seconds, a stable pattern was reached. However, in contrast to fig. 1b, approximately half (53% to be precise) of the drops remained oxidized. We note that the stable state was mainly composed of small domains of drops arranged in two different patterns. The first pattern had three-fold symmetry and is highlighted with a red circle in fig. 1c. The pattern is the complement of fig. 1b, *i.e.*, each reduced stationary drop was surrounded by six oxidized stationary drops and on average there were two oxidized drops for each reduced drop. The second pattern, with two-fold symmetry, was more of a labyrinth, highlighted with a blue circle in fig. 1c. The pattern consists of a line of

reduced drops parallel to a line of oxidized drops, resulting in a 50-50 mix of oxidized and reduced drops. The two-fold symmetric labyrinth pattern was present in a much higher proportion than the three-fold symmetric pattern.

Taken together, the data in fig. 1 demonstrated a clear trend of increasing fraction of drops in the oxidized stationary Turing state with increasing coupling strength accomplished by either reducing the drop diameter at constant malonic acid concentration, or reducing malonic acid concentration at constant drop diameter. For each experiment, the data analysis is based on at least several hundreds of drops in order to obtain good statistical accuracy. We examine this phenomenon further with numerical simulations in the next section.

### 3.2 Finite element simulation of 2D patterns

To better understand the relationship between the various Turing patterns in 2D hexagonal lattices as a function of the inhibitory coupling strength, we performed finite element modeling using COMSOL multiphysics software.

In previous work [12], a simplified point model was used for simulating 2D lattices of BZ droplets. Each drop was considered to be a single point and the oil separating drops was treated implicitly by considering a specific coupling of chemicals directly between nearest neighbors. Here we employ finite element modeling which allows for explicitly considering both the size of the drop and the amount of oil separating drops [9]. To speed up the calculation, we restricted the model to two dimensions as shown in fig. 2, which compares experiment and simulation. The same FKN theory was used in these simulations as in previous works for the equations governing chemical reactions and are included in appendix A for completeness [9, 10]. We allowed only bromine to diffuse between droplets through oil gaps in these simulations with a partition coefficient of 2.5. Bromine concentration is shown in color with bromine flux shown in black arrows. An oxidized stationary droplet has a higher bromine concentration and hence is redder than the reduced stationary drops. The color scale in oil gap is different (2.5 times higher) from that in the aqueous droplet for better appearance. The initial chemical conditions used in the simulation were chosen to be similar to the experimental initial chemical conditions. Note that these conditions are different than the steady state solutions of the reaction-diffusion equations. Random initial bromide ion concentrations were used for the drops in the unit cell so that every drop would start differently from the others. The randomness was limited to 20% of the average value of initial bromide ion concentration, 5e-5 M. The initial chemical conditions for other species in simulation were chosen to be similar to experimental initial chemical conditions, *i.e.* all catalysts were in the reduced state and the concentrations for the other species were nearly zero. Periodic boundary conditions were applied to the parallel pairs of the polygons. See Supplementary material S1 for an example of COMSOL model.

In a 2D system, the monolayer of BZ drops is arranged in hexagonal lattice, thus a hexagon unit cell was a natural choice for simulation (fig. 2b and d). The hexagon unit cell involves 7 drops, with 6 drops partly inside the cell and the center one fully inside, resulting a total of 3 full drops in the unit cell. Parallel boundaries in the hexagon cell were set to be periodic, thus the unit cell extends to an infinite 2D plane. In the first four images, fig. 2a-d, the malonic acid concentration is held constant and the drop size is varied; large drops in fig. 2a-b and small drops in fig. 2c-d. The simulation results using the hexagon unit

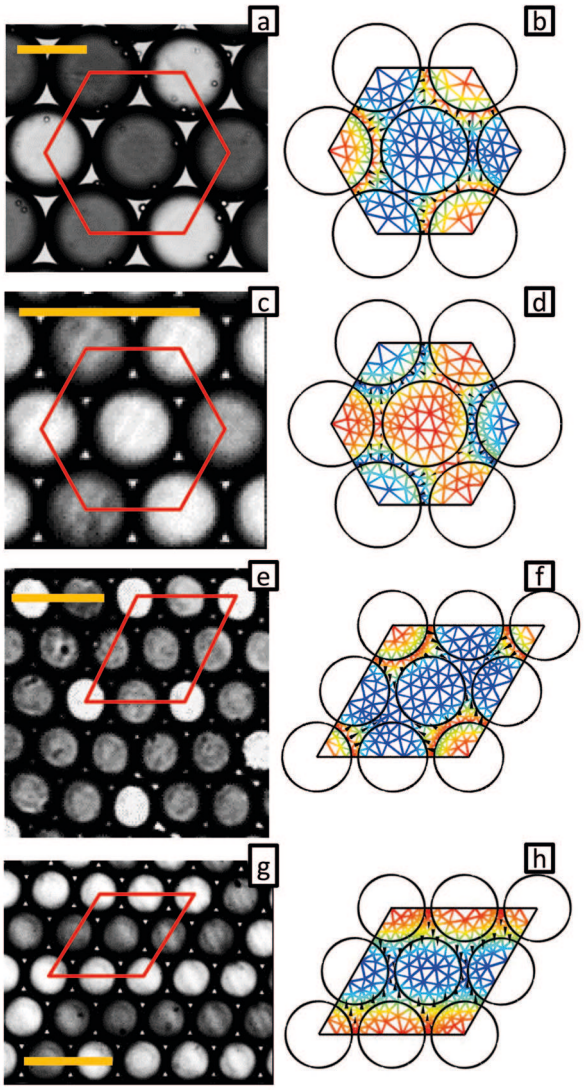


**Fig. 2.** Experimentally observed stationary chemical states and finite element simulations of BZ drops in 2D. The left-hand column (a, c, e, g) are experimental photographs. The yellow bar in each image is 100 $\mu$m long. The red polygon in each image is the unit cell that was simulated and displayed on the right-hand column. The right-hand side (b, d, f, h) are finite element calculations based on the 7-variable FKN model solved COMSOL. Bromine concentration is shown in color (orange = high, blue = low) with the bromine flux indicated by small black arrows. The small triangles in the simulations are the mesh used for calculation. The conditions for each experiment and simulation are given in table 1.

**Table 1.** Parameters in fig. 2.

| Figure | $a$ ($\mu$m) | $m$ (mM) | OST (%) |
|---|---|---|---|
| a | 120 | 200 | 33.3 |
| c | 50 | 200 | 66.7 |
| e | 50 | 400 | 25 |
| g | 50 | 200 | 50 |
| b | 100 | 40 | 33.3 |
| d | 40 | 40 | 66.7 |
| f | 40 | 100 | 25 |
| h | 40 | 40 | 50 |

cell with large drops in fig. 2b resembled the experimental pattern in fig. 2a in which 1/3 of the drops were oxidized. Likewise, the simulation results using the hexagon unit cell with small drops in fig. 2d resembled the experimental pattern in fig. 2c in which 2/3 of the drops were oxidized.

Besides patterns with three-fold symmetry, we also observed patterns with two-fold symmetry, as illustrated in figs. 2e and g. Diamond-shaped unit cells containing 4 full drops (figs. 2f and h) were used to simulate these patterns in which periodic boundary conditions were also applied. The size and symmetry of the unit cell restricts the chemical states that the drops can adopt. With the hexagonal unit cell the possibilities for the fraction of drops in the stationary oxidized state are {0, 1/3, 2/3, 1}, while with the diamond cell, the possibilities are {0, 1/4, 1/2, 3/4,1}. In order to eliminate the bias imposed by choice of the unit cell, we kept the unit cell constant and varied only one parameter at a time, *i.e.* the drop diameter or malonic acid concentration.

Next we examine the parameters controlling the coupling strength, *i.e.* malonic acid concentration $m$ and drop diameter $a$, used in experiments and simulations in fig. 2 as listed in table 1. We consider four cases involving drops in the stationary state. In figs. 2a and c, $m$ is constant at 200 mM while $a$ decreased from 120 $\mu$m (fig. 2a) to 50 $\mu$m (fig. 2c). Associated with the decrease in size is an increase in the fraction of drops in the OST state from 1/3 ($a = 120\,\mu$m) to 2/3 ($a = 50\,\mu$m). From fig. 2c to fig. 2e, the drop diameter is held constant at $a = 50\,\mu$m and $m$ is increased from 200 mM to 400 mM, leading to a decrease of OST fraction from 2/3 to 1/4. In each case, the fraction of oxidized drops increases as coupling strength, $S$, increases. Figures 2g and c were actually different parts of the same experiment, each of which are indicated by circles in fig. 1c. Finite element simulations of close-packed arrays of drops as a function of $a$ and $m$, shown in figs. 2b, d, f, and h, revealed the same trend in OST fraction as experimentally observed. The agreement between experiment and simulation was qualitative not quantitative. We speculate that the reasons for this quantitative mismatch are that simulation is done in two dimensions, instead of three and that the oil gap size in the finite element model was larger than in experiment. We simulated in 2D and set the minimum oil gap size between nearest neighboring

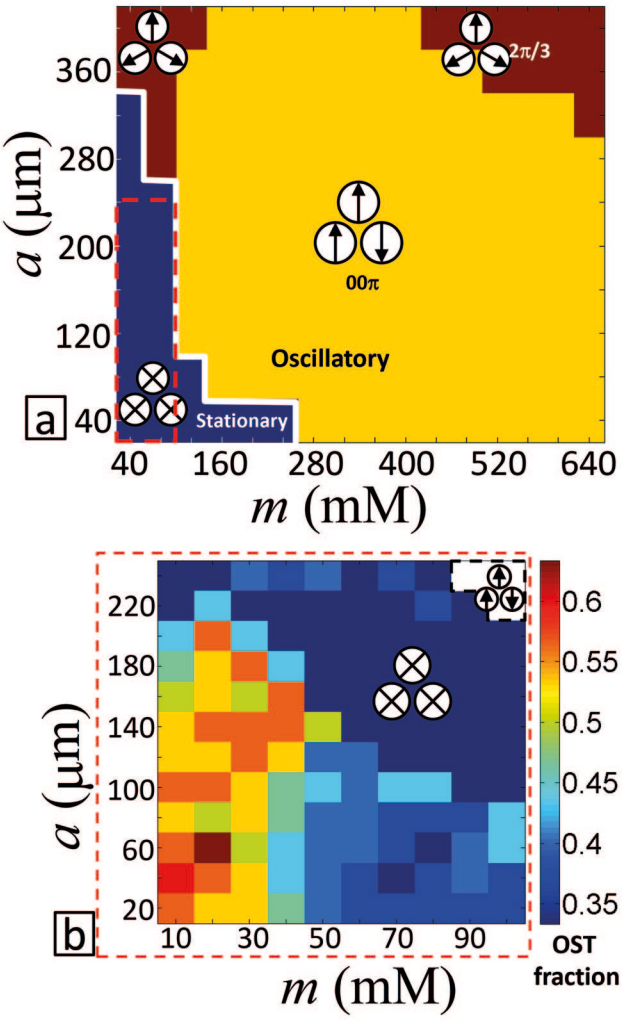


**Fig. 3.** Simulated chemical state diagram with bromine only coupling and periodic boundary conditions for a hexagonal lattice of BZ drops in 2D. (a) The model was simulated at increments of 40 mM of malonic acid concentration and in increments of 40 $\mu$m of drop diameter. Blue, yellow and dark red regions represent stationary, 00$\pi$ oscillation, and 2$\pi$/3 oscillation, respectively. Controlled initial condition was used. (b) State diagram for stationary Turing patterns. Simulations were performed at intervals of 10 mM of malonic acid and at intervals of 20 $\mu$m, with 10 trials of random initial conditions. The randomness was limited to 20% of the average value of initial bromide ion concentration, 5e-5 M. The color scale represents the fraction of oxidized stationary Turing state, *e.g.* 0.33 (dark blue) means 1/3 of the drops are oxidized.

drops to be 10% of the drop diameter instead of zero (for touching drops in experiments) in order to increase the speed of the numerical calculations. While dramatically saving computation time, these simplifications resulted in a weaker coupling strength for the simulations in comparison to the touching drops in experiments. Consequently, the simulations require smaller drop sizes and lower concentrations of malonic acid in order to produce the same patterns as observed experimentally.

In order to calculate a state diagram of the system of hexagonal close-packed BZ drops, we performed hundreds of simulations similar to the one shown in fig. 2b for a wide range of coupling strengths by varying $m$ and $a$ and the results are illustrated in fig. 3a. In the bottom left corner of the state diagram (blue region), where the coupling is the strongest, all drops in the hexagon unit cell are non-oscillating. Increasing $m$ and $a$ from the stationary region leads to the yellow region in which all three drops in the unit cell oscillate; two of the drops oscillate in-phase with each other and $\pi$ radians out of phase with the third drop. We denote this pattern "$00\pi$" meaning two drops have zero phase difference and the third beats 180 degrees out of phase with the others. Weakening coupling strength by increasing drop diameter $a$ from the stationary region leads to the dark red region, which is another pattern in which all three drops in the unit cell oscillate, but this time each drop has a 120 degrees phase shift with its two neighbors in the unit cell. We denote this pattern "$2\pi/3$". We find the same pattern in the top right corner of the diagram where the coupling is the weakest. The initial chemical conditions for each drop in the unit cell were taken from an isolated free-run drop at phase shifts of 0, 120 and 240 degrees on the limit cycle at $m = 400$ mM. Since this initial condition is the only other kind of initial condition we used for simulations besides the random initial condition, we denote it as the "controlled initial conditions" in this paper. We also numerically verified that decoupled ($P_{\mathrm{B}} = 0$) drops with conditions from the blue stationary region of the state diagram of fig. 3a would oscillate autonomously, but these oscillating drops became stationary when coupled ($P_{\mathrm{B}} = 2.5$). This phenomena has been referred to as coupling-induced oscillator death [18]. Our numerical analysis suggests that the boundary between the stationary and oscillatory border in the state diagram does not depend on initial conditions.

At this point, we make a brief comparison of simulation and experiment. Qualitatively, there is a correspondence between regions of strong and weak coupling strength. For both computation and experiment at strong coupling (small drops, low malonic acid) the drops are stationary, while at weak coupling all drops oscillate in the $2\pi/3$ state. We note that there is a significant discrepancy between the computed state diagram of fig. 3 and the experiments of fig. 1a. In experiment, for intermediate coupling strength, indicated by region II of fig. 1a we observe the $s0\pi$ state. However, in simulation this state is never observed for homogeneous drops. Instead, all drops oscillate in the $00\pi$ state, which, in spite of hundreds of experiments, was never observed in large arrays of hexagonally packed drops. The origin of this discrepancy will be explored in the section on heterogeneity.

To explore further the stationary Turing pattern and quantify the fraction of drops in the oxidized stationary Turing state as a function of coupling strength, we performed simulations with higher resolution of $m$ and $a$ in part of the blue (stationary) region indicated by the red dashed lines. Figure 3b shows the fraction of drops in the Oxidized Stationary Turing (OST) state using a different color map ranging from 1/3 (blue) to 2/3 (red). We observed that the OST fraction also depends on initial conditions to a certain degree. Consequently, we averaged the results from 10 trials of simulation at each point of the inset diagram with randomized initial concentrations of bromide ion, the actual inhibitor in aqueous phase [14,15], for each of the 3 drops in the unit cell. We can see that as $m$ increased beyond 50 mM, or once $a$ increased beyond 200 $\mu$m, the fraction of OST decreased quickly. Overall, the computations reveal that the of fraction of stationary drops in the oxidized state increases with smaller drop diameter and/or lower malonic acid concentration, *i.e.* with increased stronger coupling strength. This trend agrees qualitatively with the experiments in figs. 1 and 2.

The state diagram in fig. 3a agrees with one calculated previously using a point-oscillator model [8]. The only differences are that we considered activator coupling as well as inhibitory coupling, which produced in-phase synchronous oscillations in the limit of high coupling strength [8]. We verified that in-phase oscillations at high coupling strength occur in the finite element model when activation coupling was included. Since we never observed in-phase oscillations at high coupling strength in experiment, we only considered inhibitory coupling in this paper.

### 3.3 Heterogeneity in mixed patterns

There are two qualitative differences between the simulated phase diagram and the experiments; the absence of the $s0\pi$ state in simulations and the absence of the $00\pi$ state in the experiments, which we will see are linked. In spite of a large number of attempts using a wide range of parameters, simulations of a hexagon unit cell composed of identical BZ drops lack a mixed oscillatory and stationary state, such as the experimentally observed $s0\pi$ state in fig. 1a, region II. What we found instead in simulation in the regions where experiment gave the $s0\pi$ state was a state in which all drops in a unit cell oscillated in the $00\pi$ state. As mentioned in previous work [8], some heterogeneity must be introduced to either the geometry (*i.e.* the drop diameter or interdrop spacing), or in the chemistry of the drops in order for the simulations to generate mixed oscillatory and stationary patterns that resemble the experimentally observed patterns. Experimentally we tried to make the drops as uniform as possible. The diameters varied by less than 2%. It was harder to determine the variance in chemical composition. We did measure the period of individual drops and found that the periods varied by 3% [8].

In fig. 4 we employ finite element calculations to numerically explore the effect of heterogeneity in chemistry, specifically the acidity [$H^+$] in BZ drops. The oscillation frequency increases rapidly with increasing acidity [14,15]. The simulation employed a hexagonal unit cell consisting of three drops of identical diameter with periodic boundary conditions, such as shown in fig. 2b. Each of the three

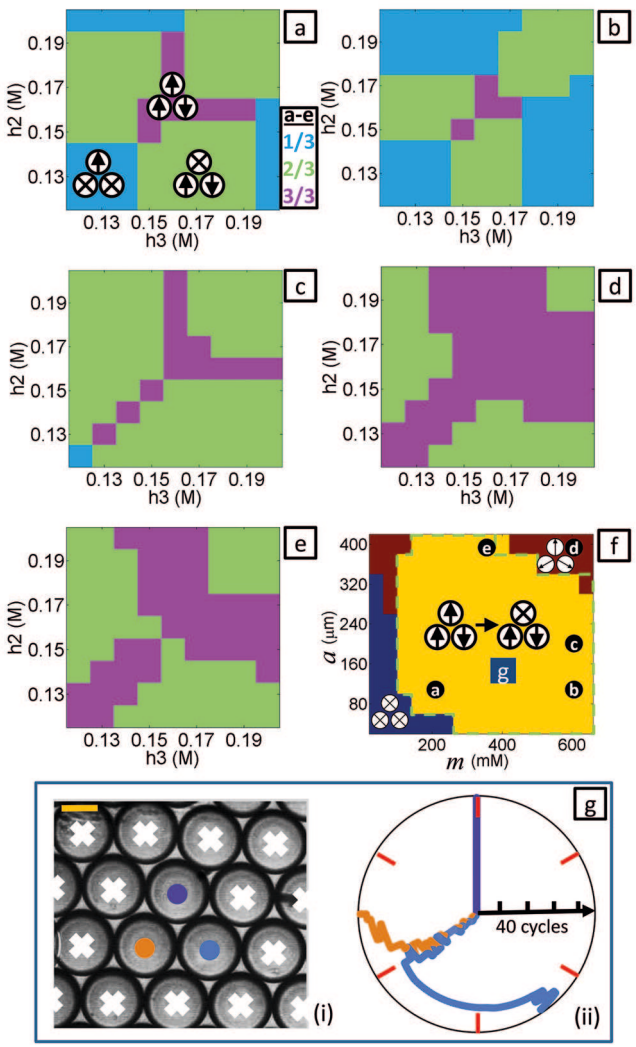


**Fig. 4.** Effect of chemical heterogeneity on the states of BZ drops in hexagonal lattices. (a)–(e) are the fraction of drops that oscillate, calculated with parameters $m$ and $a$ as indicated in the phase diagram (f), the same phase diagram as portrayed in fig. 3. The same finite element module and controlled initial condition was used for the simulations in (a)–(e) as in the phase diagram (f). The light blue region in (a)–(e) represents patterns with 1/3 of drops oscillating; light green region with 2/3 of drops oscillating; purple region for all (3/3) drops oscillating. The light green dashed line in phase diagram (f) marks the region of $s0\pi$ pattern with $h_2 = 0.15\,\mathrm{M}$ and $h_1 = h_3 = 0.16\,\mathrm{M}$, which is almost identical to the yellow region of $00\pi$ for homogeneous drops. (g(i)) is a photograph of three optically isolated drops and is the closest experimental observation of the $00\pi$ pattern. The drops with "×" had light shone on them, which sets those drops in the reduced, stationary state [8]. The yellow bar is $100\,\mu\mathrm{m}$ long. (g(ii)) is a radial space-time plot with the time axis radial with a length corresponding to 40 oscillations. The polar angles mark the relative phase shift between oscillating drops. The color coding identifies the drops in g(i). The phase shift is plotted relative to the purple drop and the phase of the purple drop is fixed at zero degrees.

drops in a unit cell are allowed to have different values of $[H^+]$: $h_1$, $h_2$, $h_3$. We let two of these three values, *i.e.* $h_2$ and $h_3$, vary from 0.12 M to 0.2 M in increments of 0.01 M and leave one drop, $h_1$, fixed at 0.16 M. In figs. 4a to e, we vary the drop size $a$ and malonic acid concentration $m$, the two parameters that most strongly control the coupling strength. The values of $m$ and $a$ used in figs. 4a-e are indicated by the corresponding letter in fig. 4f. From the strongest coupling in fig. 4a to the weakest coupling in fig. 4d we noticed the trend of increasing area of the fully oscillatory domain in purple, as well as the trend of diminishing area of the blue domain where only one third of the drops oscillate. All non-oscillating drops were effectively in the reduced stationary state, although they were actually oscillating with a very small amplitude that was only observable in numerical simulations. The minimum amounts of heterogeneity in $[H^+]$ needed for $s0\pi$ state were 0.01 M (*i.e.* 1/16) for cases a, b, c, e and 0.02 M (1/8) for case d.

In fig. 4f we recalculated the phase diagram with the minimum heterogeneity in $h_2$ so that $h_1 = h_3 = 0.16\,\mathrm{M}$ and $h_2 = 0.15\,\mathrm{M}$. The result was nearly identical to the homogeneous case in which all drops had the same acidity, $h_1 = h_2 = h_3 = 0.16\,\mathrm{M}$, shown in fig. 3, except that almost all of the $00\pi$ pattern denoted by a yellow region in fig. 3 transformed to the $s0\pi$ pattern as indicated by the yellow color and light green dashed line in fig. 4f. The simulation agrees with what we found in experiments (fig. 1a region II) in that $s0\pi$ pattern occurs at medium coupling strength.

The $00\pi$ state observed in the simulated state diagram of perfectly identical drops, shown in fig. 3, was never observed in experiments on large arrays of drops, which contain both chemical and physical heterogeneities. However, there was one experimental example that resembled the $00\pi$ state, which was for the case of a triplet of drops isolated from the rest by using light to impose constant chemical conditions [8]. In this singular example, two drops oscillated in phase with each other and the third drop oscillated $2\pi/3$ out of phase. Figure 4g shows our observation of the $00\pi$ state in a system with $m = 400\,\mathrm{mM}$ and $a = 150\,\mu\mathrm{m}$, as indicated in figs. 4(f) with a blue "g". Three times of the typical $Ru(bipy)_3$ concentration was used in this particular experiment. In fig. 4g(i) the drops marked with a white "×" are optically inhibited creating constant chemical boundary conditions for the three drops in a triangle indicated with colored circles. Videos of the $00\pi$ state are shown in Supplementary movies S6 and S7. Figure 4g(ii) presents a radial-phase-time plot of the three drops in fig. 4g(i). Time starts at the center of the plot along the radial axis and the phase relative to the purple drop is shown on the angular axis. The whole experiment was approximately 3 hours long and contained 40 oscillations for each drop. For approximately 35 oscillations the orange and blue drops are synchronized with zero relative phase and approximately $2\pi/3$ out of phase to the purple drop. Eventually the "$00\pi$" state decays into the $2\pi/3$ phase state.

## 4 Conclusions

The main conclusions are:

1. Both reaction and diffusion mediate the coupling strength through the dimensionless parameter $S = \mu/k_{\text{eff}}$, with $\mu = \alpha P_{\text{B}} D/a^2$ the term involving diffusion and $k_{\text{eff}} \propto m$ the term involving chemistry. Chemically, increasing $m$ increases bromine consumption *via* the bromination of malonic acid inside a drop. Any bromine diffusing into a drop with high $m$ is consumed instead of increasing the bromine concentration and thereby the coupling strength is weak. Physically, increasing $a$ increases the time for bromine to diffuse from one drop to another and thereby gives the bromine more time to react with the malonic acid. Thus the bromine in a large drop is less likely to diffuse to a neighboring drop before it is consumed. When $m$ and $a$ are small enough, the diffusive lateral inhibition becomes strong enough to induce oscillator death and cause stationary patterns to emerge in 2D systems. A stationary drop can be either oxidized stationary that is continuously emitting bromine, or reduced stationary that is continuously being inhibited. As $m$ or $a$ are decreased further, the diffusive lateral inhibition gets even stronger. This led to an increase in the number of stationary drops in the oxidized state and a decrease in the number in the reduced state; in other words, more drops were doing the inhibiting and fewer drops were inhibited.

2. Finite element methods provide the highest accuracy for simulations of reaction-diffusion systems in complex geometries. This level of accuracy is necessary to properly simulate our 2D systems, at the price of higher computational power and longer computing time compared to simplified point models. Using the finite element model we have simulated patterns resembling all the stationary patterns we found in experiments. Over a wide range of coupling strength we generated a simulated state diagram that agreed qualitatively with experiments. The trend of increasing fraction of oxidized stationary drops with increasing coupling strength, observed in experiment, was also found in simulations. We performed simulations with various combinations of coupling species and the best results are obtained when the coupling is through only bromine.

The current finite element model can be improved for better quantitative agreement with experiments in the future by allowing the drops to touch, and by constructing a fully 3D geometry. Moreover, a larger unit cell would provide insight on the effect of diffusion beyond that of nearest neighbors.

3. Microfluidic devices generate physically and chemically monodispersed BZ droplets with only a few percent of variance. We demonstrated that a few percent of chemical variance in simulations ($\sim 6\%$ in acidity, which controls the oscillatory frequency) was enough to generate the $s0\pi$ pattern, which in spite of great effort, was never found in simulations employing identical drops. In contrast, the $00\pi$ pattern that appeared in simulations of homogeneous arrays of drops was never experimentally observed in large arrays of drops for which, inevitably, there was some heterogeneity in the lattice and hence in the coupling strength. It would be interesting to systematically investigate the effect of heterogeneity in the future by deliberating varying the physical size, chemical composition, and positions of individual drops in a variety of two-dimensional lattices and networks.

We appreciate the help from Dr. Francesco Pontiggia on cluster computing. We acknowledge support from the Brandeis University NSF MRSEC, DMR-1420382 and use of the MRSEC microfluidics facility.

## Appendix A. FKN mechanism

Field, Körös and Noyes published a series of fundamental works in the 1970's offering a detailed mechanism of the BZ oscillation [14,15], later known as the FKN mechanism. All of our simulations are based on this mechanism, sometimes with minor variances [16,17]. FKN treats the complete BZ cycle as the result of three processes. In process A, there is sufficient bromide ion in an acid solution of bromate and malonic acid to suppress Process B. The sequence (A.1) + (A.2) + 3(A.3) + 3(A.4) results in net process A (A.5).

### Process A

$$\text{BrO}_3^- + \text{Br}^- + 2\text{H}^+ \xrightarrow{k_2} \text{HBrO}_2 + \text{HOBr}, \tag{A.1}$$

$$\text{HBrO}_2 + \text{Br}^- + \text{H}^+ \xrightarrow{k_1} 2\text{HOBr}, \tag{A.2}$$

$$\text{HOBr} + \text{Br}^- + \text{H}^+ \underset{k_6}{\overset{k_5}{\rightleftharpoons}} \text{Br}_2 + \text{H}_2\text{O}, \tag{A.3}$$

$$\text{Br}_2 + \text{CH}_2(\text{COOH})_2 \xrightarrow{k_7} \text{BrCH(COOH)}_2 + \text{Br}^- + \text{H}^+, \tag{A.4}$$

Net process A:

$$\text{BrO}_3^- + 2\text{Br}^- + 3\text{CH}_2(\text{COOH})_2 + 3\text{H}^+ \rightarrow 3\text{BrCH(COOH)}_2 + 3\text{H}_2\text{O}. \tag{A.5}$$

When bromide ion is virtually absent, bromate ion reacts with the catalyst (Ce(III) in the original paper [14], Fe(II) in our case) and malonic acid. The sequence 2(A.6) + 4(A.7) + (A.8) + (A.9) results in the net process B (A.10). The sequence (A.6) + 2(A.7) leads to autocatalytic production of $\text{HBrO}_2$.

### Process B

$$\text{BrO}_3^- + \text{HBrO}_2 + \text{H}^+ \underset{k_r}{\overset{k_4}{\rightleftharpoons}} 2\text{BrO}_2\cdot + \text{H}_2\text{O}, \tag{A.6}$$

$$\text{BrO}_2\cdot + \text{Fe(phen)}_3^{2+} + \text{H}^+ \xrightarrow{k_{\text{red}}} \text{HBrO}_2 + \text{Fe(phen)}_3^{3+}, \tag{A.7}$$

$$2\text{HBrO}_2 \xrightarrow{k_3} \text{BrO}_3^- + \text{HOBr} + \text{H}^+, \tag{A.8}$$

$$\text{HOBr} + \text{CH}_2(\text{COOH})_2 \xrightarrow{k_8} \text{BrCH(COOH)}_2 + \text{H}_2\text{O}, \tag{A.9}$$

Net process B:

$$\mathrm{BrO_3^-} + 4\mathrm{Fe(phen)_3^{2+}} + \mathrm{CH_2(COOH)_2} + 5\mathrm{H^+} \rightarrow \mathrm{BrCH(COOH)_2} + 4\mathrm{Fe(phen)_3^{3+}} + 3\mathrm{H_2O}. \quad \text{(A.10)}$$

The irreversible processes A and B take place under different conditions in the same system and a solution reacting by process A will eventually convert itself to one reacting by process B. To have oscillation, however, we need to get back from B to A. This is accomplished by Fe(III) produced in process B reacting with the organic species by overall processes (A.11) and, more importantly (A.12). When the rate of (A.12) becomes sufficiently great, process B is "turned off" and process A is re-initiated, so that the oscillatory cycle and begin again. The net process C is the result of the sequence $x$(A.5) + $(3-x)$(A.10) + $(2-2x)$(A.11) + $2x$(A.12) where $x \in [0,1]$.

### Process C

$$6\mathrm{Fe(phen)_3^{3+}} + \mathrm{CH_2(COOH)_2} + 2\mathrm{H_2O} \xrightarrow{k_{10}} 6\mathrm{Fe(phen)_3^{2+}} + \mathrm{HCOOH} + 2\mathrm{CO_2} + 6\mathrm{H^+}, \quad \text{(A.11)}$$

$$4\mathrm{Fe(phen)_3^{3+}} + \mathrm{BrCH(COOH)_2} + 2\mathrm{H_2O} \xrightarrow{k_9} \mathrm{Br^-} + 4\mathrm{Fe(phen)_3^{2+}} + \mathrm{HCOOH} + 2\mathrm{CO_2} + 5\mathrm{H^+}. \quad \text{(A.12)}$$

Net process C:

$$3\mathrm{BrO_3^-} + 5\mathrm{CH_2(COOH)_2} + 3\mathrm{H^+} \rightarrow 3\mathrm{BrCH(COOH)_2} + 2\mathrm{HCOOH} + 4\mathrm{CO_2} + 5\mathrm{H_2O}. \quad \text{(A.13)}$$

### Reactions with light

To have light control of BZ oscillation we need to use $\mathrm{Ru(bipy)_3}$. In principle we can use $\mathrm{Ru(bipy)_3}$ only. However, to improve optical contrast, we also use ferroin. The photosensitive reactions involving Ru(II) complex (*i.e.* $\mathrm{Ru(bipy)_3^{2+}}$) are listed here [16]

$$\mathrm{Ru(bipy)_3^{2+}} + h\nu \xrightarrow{k_\mathrm{I}} \mathrm{Ru(bipy)_3^{2+}}*, \quad \text{(A.14)}$$

$$\mathrm{Ru(bipy)_3^{2+}}* + \mathrm{BrCH(COOH)_2} + \mathrm{H^+} \xrightarrow{k_\mathrm{C}} \mathrm{Ru(bipy)_3^{3+}} + \mathrm{Br^-} + \text{products}, \quad \text{(A.15)}$$

$$\mathrm{Ru(bipy)_3^{2+}}* \xrightarrow{k_\mathrm{d}} \mathrm{Ru(bipy)_3^{2+}}. \quad \text{(A.16)}$$

### Differential equations for reaction

We summarized the constant and variable chemical species and the reaction rates for the full FKN model in table 2. With the variables and constants defined in this table, we have the set of ordinary differential eqs. (A.17) to (A.23) derived from reactions (A.1) to (A.16).

For light controlled reactions, $k_\mathrm{I} = 10^{-3} \sim 10^{-4}\,\mathrm{s^{-1}}$, $b_\mathrm{C} = k_\mathrm{d}/k_\mathrm{C} = 0.05\,\mathrm{M}$. While we use two catalysts $\mathrm{Fe(phen)_3}$ and $\mathrm{Ru(bipy)_3}$ in our experiments, in simulation we disregard this distinction and consider only one photosensitive catalyst represented by $c/z$ in its reduced/oxidized form

$$\frac{\mathrm{d}x}{\mathrm{d}t} = -k_1xy + k_2y - 2k_3x^2 - k_4x + k_\mathrm{r}w^2 + k_\mathrm{red}wc, \quad \text{(A.17)}$$

$$\frac{\mathrm{d}y}{\mathrm{d}t} = -k_1xy - k_2y - k_5yp + k_6u + k_7u + k_9z + \frac{k_\mathrm{I}cB}{b_\mathrm{C}+B}, \quad \text{(A.18)}$$

$$\frac{\mathrm{d}z}{\mathrm{d}t} = k_\mathrm{red}wc - k_9z - k_{10}z + \frac{k_\mathrm{I}cB}{b_\mathrm{C}+B}, \quad \text{(A.19)}$$

$$\frac{\mathrm{d}p}{\mathrm{d}t} = 2k_1xy + k_2y + k_3x^2 - k_5yp + k_6u - k_8p, \quad \text{(A.20)}$$

$$\frac{\mathrm{d}u}{\mathrm{d}t} = k_5yp - k_6u - k_7u, \quad \text{(A.21)}$$

$$\frac{\mathrm{d}w}{\mathrm{d}t} = 2k_4x - 2k_\mathrm{r}w^2 - k_\mathrm{red}wc, \quad \text{(A.22)}$$

$$\frac{\mathrm{d}c}{\mathrm{d}t} = -k_\mathrm{red}wc + k_9z + k_{10}z - \frac{k_\mathrm{I}cB}{b_\mathrm{C}+B}. \quad \text{(A.23)}$$

## Appendix B. Supplement S1: COMSOL example

The COMSOL file "comsol44_hex3pbc_240um.mph" in the Supplementary material can only be opened with the latest version of COMSOL multiphysics 4.4. A powerful desktop computer with at least 4GB RAM is recommended for testing the model.

This example was made with 2D diffusion module in COMSOL with periodic boundary conditions. The partition coefficient on drop-oil boundary was enforced using the stiff-spring method which is demonstrated in the model "Separation through dialysis", a built-in model example in COMSOL.

This model is already solved for 2e4 seconds (stored solution at every 1e3 seconds) with malonic acid concentration $m = 0.05\,\mathrm{M}$ and drop size $a = 240\,\mu\mathrm{m}$. Parameters such as $m$ can be modified in "Parameters" under "Global Definitions". Computation time and recorded time steps can also be modified in "Step 1: Time Dependent" under "Study 1". If you want to run the simulation with different parameters, simply click "compute" icon (the green equal sign) in "Study 1" from the model builder panel after changing parameters. Once the computation is done, the results can be plotted from "Results" panel. Concentration variables $c_1 - c_7$ are ordered as $x$, $y$, $z$, $p$, $u$, $w$, $c$ in appendix A. $c_8$ and $c_9$ are the corresponding concentration of $u$ and $w$ in oil phase. $c_0$ is light intensity expressed as pseudo concentration, which was set to zero for this simulation.

**Table 2.** Summary of chemical concentrations and reaction rates.

| Concentration | Constant | Reaction rate | Value |
|---|---|---|---|
| $[H^+]$ | $h$ | $k_1$ | $2 \times 10^6$ $[M^{-2}s^{-1}]h$ |
| $[BrO_3^-]$ | $A$ | $k_2$ | 2 $[M^{-3}s^{-1}]h^2A$ |
| $[CH_2(COOH)_2]$ | $m$ | $k_3$ | 3000 $[M^{-1}s^{-1}]$ |
| $[BrCH(COOH)_2]$ | $B(=0.1m)$ | $k_4$ | 42 $[M^{-2}s^{-1}]hA$ |
| Concentration | Variable | $k_5$ | $5 \times 10^9$ $[M^{-2}s^{-1}]h$ |
| $[HBrO_2]$ | $x$ | $k_6$ | 10 $[s^{-1}]$ |
| $[Br^-]$ | $y$ | $k_7$ | 29 $[M^{-1}s^{-1}]m$ |
| [HOBr] | $p$ | $k_8$ | 9.3 $[M^{-1}s^{-1}]m$ |
| $[BrO_2\cdot]$ | $w$ | $k_9$ | 0.07–0.12 $[M^{-1}s^{-1}]m$ |
| $[Br_2]$ | $u$ | $k_{10}$ | 0.05 $[M^{-1}s^{-1}]m$ |
| $[Fe(phen)_3^{2+}]$ | $c$ | $k_r$ | $2 \times 10^8$ $[M^{-1}s^{-1}]$ |
| $[Fe(phen)_3^{3+}]$ | $z$ | $k_{red}$ | $5 \times 10^6$ $[M^{-1}s^{-1}]$ |

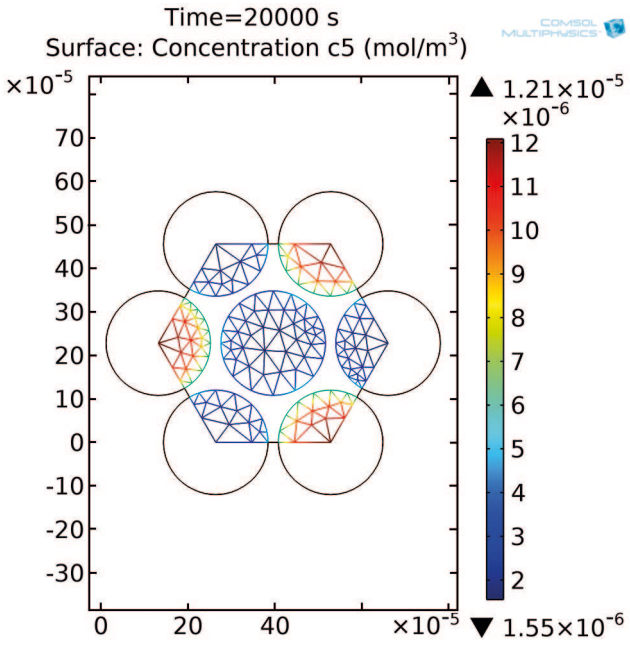


**Fig. 5.** Example of COMSOL simulation result. The color scale indicates bromine concentration in the drops after the system reached the stable stationary state at $t = 20000$ s.

In fig. 5 (*i.e.* Supplementary figure S1) we show the stored solution of bromine concentration ($c_5$) in the example file. The color scale indicates bromine concentration in the drops after the system reached the stable stationary state at $t = 20000$ s, which is the Oxidized-Reduced-Reduced stationary Turing pattern we discussed in the main text.

## Appendix C. Supplement S2-S7: Video captions

– S2: The movie shows the full field of view of the capillary with thousands of BZ drops as described in fig. 1b, from $t = 0$ to $t = 1000$ s. The video is 40 times faster than real time. Initially the drops are in the reduced state, inhibited by bromide that was added when the drops were created. The drops all simultaneously oxidize, but the synchrony is not a result of coupling, but because the drops were all created at the same time. With time the drops adopt a pattern of three-fold symmetry with one drop oxidized for two reduced drops.

– S3: Close-packed BZ emulsion demonstrating the $2\pi/3$ attractor state. Any triangle of drops oscillates in either a left-handed or right-handed pattern with a $2\pi/3$ phase difference between neighbors. Each drop is approximately 150 $\mu$m in diameter in a 100 $\mu$m tall capillary and the movie is sped up 200 times. Chemical conditions: 80 mM $H_2SO_4$, 300 mM Bromate, 10 mM NaBr, 640 mM MA, 3 mM Ferroin, 0.4 mM Rubpy.

– S4: Close-packed BZ emulsion demonstrating the $2\pi/3$ attractor state. Any triangle of drops oscillates in either a left-handed or right-handed pattern with a $2\pi/3$ phase difference between neighbors. Every drop is individually tracked and labelled. The color of the circle indicates the $2\pi/3$ order parameter for the upright triangle of drops which that drop is at the top of. A right-handed pattern is colored red and a left-handed pattern is colored blue with the intensity of the color corresponding to how perfectly $2\pi/3$ the phase differences are. A green circle indicates one of the three drops in the triangle has not yet oscillated and a white circle indicates an incomplete

triangle. Each drop is approximately 150 $\mu$m in diameter in a 100 $\mu$m tall capillary and the movie is sped up 200 times. Chemical conditions: 80 mM $H_2SO_4$, 300 mM Bromate, 10 mM NaBr, 640 mM MA, 3 mM Ferroin, 0.4 mM Rubpy.

– S5: Close-packed BZ emulsion demonstrating the $2\pi/3$ attractor state. A single triangle of drops oscillating in a left-handed pattern with a $2\pi/3$ phase difference between neighbors. Each drop is approximately 150 $\mu$m in diameter in a 100 $\mu$m tall capillary and the movie is sped up 200 times. Chemical conditions: 80 mM $H_2SO_4$, 300 mM Bromate, 10 mM NaBr, 640 mM MA, 3 mM Ferroin, 0.4 mM Rubpy.

– S6: Three optically isolated drops demonstrating the $00\pi$ state. Every drop except for the three oscillating drops in the middle is being inhibited with blue light. The inhibitory light is not visible due to time-multiplexing. Each drop is approximately 150 $\mu$m in diameter in a 100 $\mu$m tall capillary and the movie is sped up 100 times. Chemical conditions: 80 mM $H_2SO_4$, 300 mM Bromate, 10 mM NaBr, 400 mM MA, 3 mM Ferroin, 1.2 mM Rubpy.

– S7: Three optically isolated drops demonstrating the $00\pi$ state with a phase plot movie. Every drop except for the three color coded drops in the middle is being inhibited with blue light. The inhibitory light is not visible due to multiplexing. The phases of the three color-coded drops are plotted on the phase circle. The phase circle is in a moving reference frame rotating at the average frequency where the white dot is phase zero. Every time the white dot crosses a colored circle that drop flashes. Each drop is approximately 150 $\mu$m in diameter in a 100 $\mu$m tall capillary and the movie is sped up 33 times. Chemical conditions: 80 mM $H_2SO_4$, 300 mM Bromate, 10 mM NaBr, 400 mM MA, 3 mM Ferroin, 1.2 mM Rubpy.

## References


1. A.M. Turing, Philos. Trans. R. Soc. London **237**, 37 (1952).
2. K.U. Torii, Trends Cell Biol. **22**, 438 (2012).
3. M. Cohen, B. Baum, M. Miodownik, J. R. Soc. Interface **8**, 787 (2011).
4. P. Formosa-Jordan, M. Ibñaes, J. Stat. Mech. **2009**, P03019 (2009).
5. A.D. Economou, A. Ohazama, T. Porntaveetus, P.T. Sharpe, S. Kondo, M.A. Basson, A. Gritli-Linde, M.T. Cobourne, J.B.A. Green, Nat. Genet. **44**, 348 (2012).
6. R. Phillips, J. Kondev, J. Theriot, H. Garcia, *Physical Biology of the Cell*, 2nd edition (Garland Science, 2012).
7. F. Sagués, I.R. Epstein, Dalton Trans. **7**, 1201 (2003).
8. N. Tompkins, N. Li, C. Girabawe, M. Heymann, G.B. Ermentrout, I.R. Epstein, S. Fraden, Proc. Natl. Acad. Sci. U.S.A. **111**, 4397 (2014).
9. N. Li, J. Delgado, H.O. Gonzalez-Ochoa, I.R. Epstein, S. Fraden, Phys. Chem. Chem. Phys. **16**, 10965 (2014).
10. J. Delgado, N. Li, M. Leda, H.O. Gonzalez-Ochoa, S. Fraden, I.R. Epstein, Soft Matter **7**, 3155 (2011).
11. M. Toiya, V.K. Vanag, I.R. Epstein, Angew. Chem. Int. Ed. **47**, 7753 (2008).
12. M. Toiya, H.O. Gonzlez-Ochoa, V.K. Vanag, S. Fraden, I.R. Epstein, J. Phys. Chem. Lett. **1**, 1241 (2010).
13. C. Holtze, A.C. Rowat, J.J. Agresti, J.B. Hutchison, F.E. Angile, C.H.J. Schmitz, S. Koster, H. Duan, K.J. Humphry, R.A. Scanga *et al.*, Lab Chip **8**, 1632 (2008).
14. R.M. Noyes, R. Field, E. Körös, J. Am. Chem. Soc. **94**, 1394 (1972).
15. R.J. Field, E. Körös, R.M. Noyes, J. Am. Chem. Soc. **94**, 8649 (1972).
16. V.K. Vanag, I.R. Epstein, J. Chem. Phys. **131**, 104512 (2009).
17. V.K. Vanag, I.R. Epstein, Phys. Rev. E **84**, 066209:1 (2011).
18. D.G. Aronson, G.B. Ermentrout, N. Kopell, Physica D **41**, 403 (1990).